PAPER

Check for updates

Palladium nanoparticles loaded on nitrogen and boron dual-doped single-wall carbon nanohorns with high electrocatalytic activity in the oxygen reduction reaction†

Xueyou Tan,[a] Jinxuan Zhang,[b] Xiaohui Wu,[a] Yuanyuan Wang,[a] Meixian Li [iD][b] and Zujin Shi [iD] *[a]

Palladium nanoparticles with a diameter of 2–4 nm supported on nitrogen and boron dual-doped single-wall carbon nanohorns (Pd-NBCNHs) are synthesized *via* a one-step method and their electrocatalytic activities are investigated for the oxygen reduction reaction (ORR) in alkaline media. The electrochemical results demonstrate that the oxygen reduction peak potential of Pd-NBCNHs is similar to that of commercial 20% Pt–C. Furthermore, Pd-NBCNHs show a more positive half-wave potential than 20% Pt–C and display better long-term stability and resistance to methanol than 20% Pt–C, which is attributed to the synergetic effect of the Pd nanoparticles and NBCNHs. As NBCNHs have abundant pyrrolic nitrogen, charged sites and defective structures, they not only act as a carrier, but also provide the active sites for oxygen adsorption during the oxygen reduction reaction process. The outstanding electrochemical performance makes Pd-NBCNHs promising to be applied in fuel cells.

Introduction

Fuel cell technology, providing clean and sustainable power, has been regarded as a promising solution towards the rising global energy demand.[1–3] A highly efficient catalyst for the cathodic oxygen reduction reaction (ORR) in fuel cells is the key to achieve high energy conversion efficiency.[4] Pt-based catalysts have been conventionally considered to be the best electro-catalysts.[5] However, Pt-based catalysts suffer from poor methanol durability and long-term stability.[6] Recently, Guo and coworkers have reported a class of stable PtFe–Fe$_2$C Janus-like nanoparticle interface catalysts with unrevealed barrier-free interface electron-transfer properties for greatly boosting the ORR catalytic activity and stability.[7] But the high cost and limited resource of Pt metal still hinder its commercial applications.[8] Thus, efforts are needed to develop alternative catalysts that show comparable or even better catalytic activity than Pt.

Pd and Pt are in the same group and hence share similar electronic properties. Indeed, Pd shows favourable activity for ORR despite the superior performance of Pt.[9] But the cost of Pd

is only 1/2–1/4 of Pt, which makes Pd an attractive alternative to Pt.[10] In order to improve the ORR activity and reduce the amount of Pd, Pd-based alloyed (Pd–M, M = Co,[11–13] Fe,[12] Ni,[12,13] Sn,[14] Cu,[15,16] *et al.*) catalysts have been developed. However, some of these alloyed catalysts exhibited poor stability as a result of the dissolution or agglomeration of alloyed metal during the electrolysis process. This issue has been overcome with the development of carbon nanomaterials[17] (graphene (G), graphene oxide (GO), carbon nanotube (CNTs), *et al.*) due to their extraordinary electrical conductivity, stability and large specific area while being used as electric catalyst supports.[18] For example, Pd or Pd-based alloy supported on carbon materials, such as G-PdAu@Pd,[19] ER/PdCo-tGO[20] and Pd-PEDOT/rGO,[21] have been investigated to demonstrate improved ORR activity and sustainable stability. However, the smoothness of the surface of these carbon materials will make the interaction between the active site and the carrier too weak. In many cases, defects are actually responsible for many electrochemical activities ascribed to graphitic materials.[22,23] The defects and irregular structures of graphene could be produced by doping heteroatoms, such as N and B atoms. However, the preparation of N and B dual-doped graphene require either a complicated two-step process or the use of metal catalysts, which is extraordinarily tedious and expensive for mass production.[24–30] In addition, the existence of some unnecessary by-products and difficult-to-remove metal-impurities make it difficult to identify the nature of proposed synergistic effects.[31]

[a]Beijing National Laboratory for Molecular Science, State Key Lab of Rare Earth Materials Chemistry and Applications, College of Chemistry and Molecular Engineering, Peking University, Beijing 100871, P. R. China. E-mail: zjshi@pku. edu.cn
[b]Beijing National Laboratory for Molecular Sciences, College of Chemistry and Molecular Engineering, Peking University, Beijing 100871, P. R. China

Single-walled carbon nanohorn (CNH), is a new type of carbon nanomaterial that can be mass produced by the arc method without the metal catalysts.[32] The most distinctive feature of CNH is its "dahlia flower"-like morphology formed *via* aggregation of the angled structure, resulting in more defects and nanoscale pores that disperse the metal nanoparticles (NPs) and prevent the aggregation of metal NPs.[33,34] Compared to graphene, the inherent defect structure of CNHs may be more favorable for adsorbing oxygen and promote the oxygen reduction reaction. Moreover, CNHs can increase the amount of defects by *in situ* doping of heteroatoms without the using of the metal catalyst.[35] Furthermore, the dual-doping could disrupt the electroneutrality of graphitic π-system in carbon materials and enhance the catalytic activity to a far extent due to the synergistic effect between the doped atoms.[24] The experimental results and density functional theory (DFT) calculations show that the dopants have a lower (as B) or a higher (as N) electronegativity than that of carbon, could create charge (B^+ or C^+) sites favorable for O_2 adsorption to facilitate the ORR process.[36,37] Therefore, N and B dual-doped single-wall carbon nanohorns (NBCNHs), as an emerging carbon nanomaterial, are an alternative option thanks to large-scale production *via* one-step doping *in situ* by DC arc-discharge method without using costly metal catalysts.

CNHs also exhibit good catalytic activity toward ORR because of its high electrical conductivity, good stability and methanol tolerance.[38] Our group has found that nitrogen and boron dual-doped CNHs (NBCNHs) would largely improve their catalytic activity for ORR. However, ORR activity of NBCNHs are still lower than that of commercial Pt–C with 20wt% Pt loading (20% Pt–C). Further improvement can be achieved by the assembly of two active components (Pd NPs and NBCNHs) owing to unique properties of CNHs, as well as synergistic effect. To our best knowledge, Pd NPs loaded on the different dual-atom doped CNHs remain unexplored and their catalytic properties in ORR have not been reported yet.

In this work, Pd NPs loaded on N and B atoms dual-doped single-wall carbon nanohorns (Pd-NBCNHs) were synthesized by one-step reduction method and their ORR activities were studied in alkaline media. The electrochemical measurements indicate that Pd-NBCNHs exhibits superior electrocatalytic activity with an onset potential of −0.01 V *vs.* saturated calomel electrode (SCE), similar to that of the commercial 20% Pt–C, and half-wave potential of the former is more positive than 20% Pt–C. Furthermore, Pd-NBCNHs shows better long-term durability and methanol tolerance for ORR in the alkaline media than those of commercial 20% Pt–C, which makes it promising as cathode catalyst in fuel cells.

Experiment

Synthesis of NBCNHs

Pure CNHs were prepared by DC arc-discharge method according to our previous report.[39] Boron and nitrogen dual-doped CNHs (NBCNHs) were produced by DC arc-vaporization of carbon rod that contains B_4C and melamine composites in 400 Torr pressure of CO.[38] To remove amorphous carbon, the rough NBCNHs were roasted at 430 °C for 2 h in the air, Then the obtained NBCNHs were purified by a gravitational sedimentation method to remove giant graphite-balls.

Preparation of catalysts

Pd-NBCNHs was prepared by one-step reduction method according to the previous report.[40] Briefly, 40 mg NBCNHs were dispersed in 8 mL anhydrous ethanol by sonication at room temperature for 30 minutes. Then, 2 mL of K_2PdCl_4 aqueous solution was added into the suspension gradually under ultrasonic conditions, holding for another 2 hours. Subsequently, 20 mg $NaBH_4$ in 1 mL deionized water was added for another 40 minutes. Finally, the mixture was filtered and washed with deionized water, dried in a vacuum oven at 80 °C for 12 h.

Characterization

The morphology of Pd-NBCNHs was observed by transmission electron microscopy (TEM) at an accelerating voltage of 200 kV (JEOL-2100). The Pd content in the sample was examined by inductively coupled plasma-atomic emission spectrometer (ICP, Prodigy 7). The X-ray diffraction (XRD) patterns were performed on a Rigaku MiniFlex 600 using filtered Cu Kα radiation. Raman measurements were investigated using a 530 nm laser in the back-scattering configuration on a Jobin-Yvon HR800 Spectrometer to obtain the contents of defect in Pd-NBCNHs. Thermogravimetric analysis (TGA) was recorded on a Q600 thermogravimetric analyzer (Thermal Analysis Inc., USA) from room temperature to 1000 °C at a rate of 10 °C min^{-1} under an air flow of 100 mL min^{-1}. The chemical states of elements and the content in material were tested by X-ray photoelectron spectroscopy (XPS, Axis Ultra). The specific surface area and pore-size distribution were determined using the Brunauer–Emmett–Teller (BET) method by measuring the adsorption of N_2 on an ASAP2010 volumetric adsorption analyzer.

Electrochemical measurements

All electrochemical tests were carried out with a CHI660C electrochemical workstation (CH Instrument, Chenhua Company, Shanghai, China). A standard three-electrode cell was employed with a glassy carbon electrode (GCE, 3 mm in diameter) or rotating disk electrode (RDE, 3 mm in diameter) modified with the sample as a working electrode, a saturated calomel electrode (SCE) as the reference electrode and a Pt plate as the counter electrode. For typical fabrication of Pd-NBCNHs modified electrode, 2.0 mg catalyst in 1.0 mL of anhydrous ethanol was dispersed by ultrasonication for 30 minto prepare the catalyst ink. 35 μL of the ink was dropped onto the surface of the GCE and dried ambient temperature, followed by covering a layer of 3 μL of Nafion ionomers (0.5 wt%). Cyclic voltammograms (CVs) of samples were performed in N_2- and O_2-saturated 0.1 M KOH solution. Linear sweep voltammetry (LSV) measurements were conducted at a scan rate of 10 mV s^{-1} with a glassy carbon rotating disk electrode (3 mm diameter). For comparison, Pd-CNHs,[40] Pd-BCNHs[40] and Pd-NCNHs[40] synthesized in the previous article and the commercial catalyst (20% Pt–C) were also loaded onto the GC electrode with the same

procedure. The RDE data in alkaline solution was analyzed using the Koutecky–Levich (K–L) eqn (1),[19] where j, j_k, j_d are the measured, the kinetic and diffusion-limited current densities, respectively. n is the number of exchanged electrons per O_2 molecule, F is the Faraday constant (96 486 C mol^{-1}), k is the rate constant for O_2 reduction, D_O is the diffusion coefficient of oxygen (1.9×10^{-5} cm^2 s^{-1}), ν is the kinematic viscosity of the electrolyte (0.01 cm^2 s^{-1}), C_O is the concentration of oxygen in the bulk (1.2×10^{-6} mol cm^{-3}), and ω is the rotation rate of electrode.

$$\frac{1}{j} = \frac{1}{j_k} + \frac{1}{j_d} = \frac{1}{nFkC_O} + \frac{1}{0.2nFD_O^{2/3}\nu^{-1/6}C_O\omega^{1/2}} \qquad (1)$$

Results and discussion

As shown in Fig. 1, uniform Pd NPs with a size of 2–4 nm are homogeneously dispersed on NBCNHs with "dahlia flower"-like morphology formed *via* aggregation of the angled structure. ICP measurements confirm that Pd content (wt%) in Pd-NBCNHs is 4.70 wt%. These results indicate that the Pd NPs have been loaded on NBCNHs successfully. Furthermore, the crystalline pattern of Pd-NBCNHs was identified by XRD analysis. As shown in Fig. 2A, the diffraction peak of Pd-NBCNHs at 40.11° corresponds to the (111) plane of the face-centered cubic (FCC) structure of Pd.[41] The lattice d-spacing of (111) plane of Pd calculated is approximately 0.225 nm according to the Bragg's law,[42] which is confirmed by HRTEM in Fig. 1B. The broad peak at 26.01° is assigned to the (002) facet of CNHs,[43] indicating that the CNHs are somewhat disordered rather than being ideally graphitic. This lattice distortion within the c-planes is reflected by a larger d-spacing of the (002) basal planes in the carbon
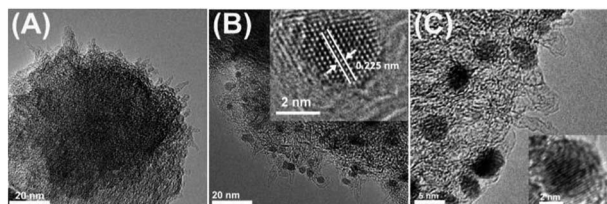

Fig. 1 TEM images of (A) NBCNHs (B) Pd-NBCNHs and (C) Pd-NBCNHs after $I–t$ chronoamperometry measurements in O_2-saturated 0.1 M KOH solutions for 9000 s. Insets show Pd NPs at a high magnification.
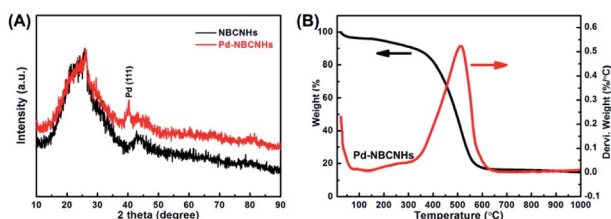

Fig. 2 (A) XRD diffraction patterns of NBCNHs and Pd-NBCNHs; (B) TGA and DTG curves of Pd-NBCNHs.
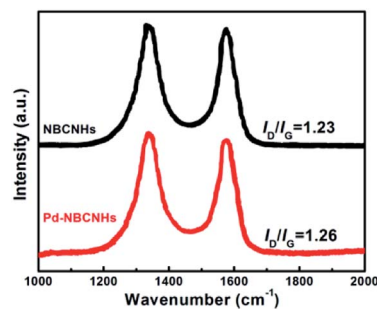

Fig. 3 Raman spectra of Pd-NBCNHs, the I_D/I_G represent the intensity ratio of D band and G band of catalysts, respectively.

relative to that in a well-ordered structure of graphite.[44] DTG curves of Pd-NBCNHs show the only characteristic peak of NBCNHs (Fig. 2B), indicating that the sample contains no other carbon impurities such as amorphous carbon or graphitic carbon.

Moreover, the surface defects of the Pd-NBCNHs were investigated by Raman spectroscopy. As shown in Fig. 3, the D band at approximately 1352 cm^{-1} and the G band at 1589 cm^{-1} represent the disordered carbon and the graphitic carbon peak, respectively.[45] The higher I_D/I_G ratio of doping carbon material implies the much more disordered carbon and defect in the sample.[46] The high I_D/I_G of Pd-NBCNHs ($I_D/I_G = 1.26$) indicates that it have more defective carbon compared with Pd-CNHs ($I_D/I_G = 1.06$),[40] suggesting that the defective carbon of CNHs increases with the introduction of heteroatom. Notably, the I_D/I_G of NBCNHs ($I_D/I_G = 1.23$) does not change significantly after loading Pd NPs. The results of Raman show that disordered carbon and defect of NBCNHs have not changed significantly after loading Pd NPs. The more defective carbon in electro-catalyst could facilitate the adsorption of oxygen molecules and breakage of O–O bond, improving the ORR activity.

The existence and content of doped heteroatoms in Pd-NBCNHs were investigated by XPS spectra. As shown in Fig. 4A, the peaks at 335.7 (Pd $3d_{5/2}$) and 341.2 (Pd $3d_{3/2}$), 337.2 (Pd $3d_{5/2}$) and 342.3 eV (Pd $3d_{5/2}$) are assigned to Pd^0 and Pd^{2+}, respectively.[47] In Fig. 4B, The B 1s peaks can be fitted into four components. The peaks at 186.4 eV, 187.7 eV, 189.7 eV and 192.5 eV are ascribed to B–C_4, B–C_3, B–CO_2 (B atoms are surrounded by carbon and oxygen atoms) and B–O structure, respectively.[48] The presence of B–C_3 structure indicates that the B atoms have been doped into the graphitic lattice in NBCNHs. The XPS spectra of N 1s of Pd-NBCNHs can be divided into four peaks, including N1 (398.6 eV, pyridinic N), N2 (400.1 eV, pyrrolic N), N3 (401.3 eV, quaternary N) and N4 (402.4 eV, pyridine-*N*-oxide) structure.[48,49] Pd-NBCNHs shows a high proportion of pyrrolic N (73.34%) that has been confirmed to play an important role in the ORR process. These results confirm that the N and B atoms have been incorporated into the corresponding carbon materials.

The ORR activity of Pd-NBCNHs was explored by cyclic voltammetry (CV) measurement. As shown in Fig. 5A, Pd-NBCNHs shows a pronounced cathodic peak at −0.190 V in O_2-saturated
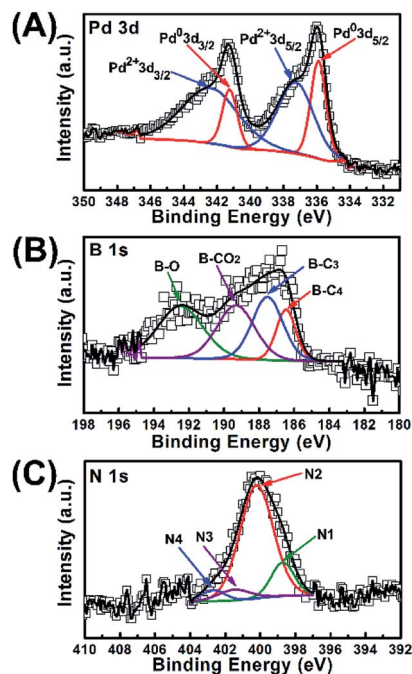
Fig. 4 (A) Pd 3d XPS spectra of Pd-NBCNHs; (B) B 1s XPS spectra of Pd-NBCNHs; (C) N 1s XPS spectra of Pd-NBCNHs.
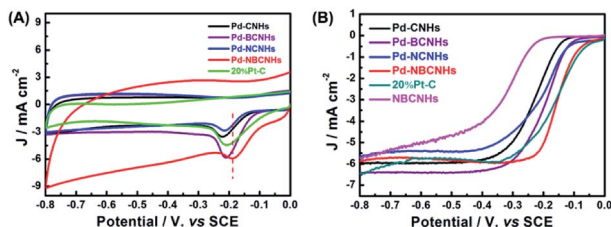

Fig. 5 (A) CV curves of samples and 20% Pt–C at 50 mV s^{-1} in O$_2$-saturated 0.1 M KOH solution; (B) LSV curves of the samples in O$_2$-saturated 0.1 M KOH solution at a rotating rate of 1600 rpm with a sweep rate of 10 mV s^{-1}.

0.1 M KOH solution, confirming a substantial ORR process (Fig. 4A). For comparison, Pd-CNHs,[40] Pd-BCNHs[40] and Pd-NCNHs[40] synthesized in the previous article were also tested using cyclic voltammetry. The ORR peak potential of Pd-CNHs, Pd-BCNHs and Pd-NCNHs are respectively at −0.221 V, −0.210 V and −0.215 V in Fig. 5A. Pd-NBCNHs shows a more positive peak potential than Pd-CNHs, Pd-BCNHs and Pd-NCNHs, indicating a better catalytic activity. It is worth mentioning that the oxygen reduction peak potential of Pd-NBCNHs is similar to that of commercial 20% Pt–C (−0.207 V, vs. SCE) in Fig. 5A. The CV result indicates that Pd-NBCNHs exhibits comparable ORR activity to that of 20% Pt–C in terms of peak potential.

Subsequently, linear sweep voltammograms (LSVs) were further performed to investigate the catalytic properties of Pd-NBCNHs and 20% Pt–C. The onset and half-wave potential are the main parameters to measure the catalytic performance of the material. The more positive onset and half-wave potential demonstrate the smaller overpotential and higher catalytic
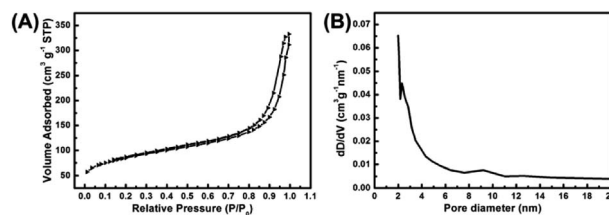

Fig. 6 (A) N$_2$ adsorption–desorption isotherms and (B) corresponding Barrett–Joyner–Halenda (BJH) pore-size distribution curve determined from the desorption branch of the isotherm of Pd-NBCNHs.

activity of catalyst toward ORR. As shown in Fig. 5B, Pd-NBCNHs exhibits an onset potential (−0.01 V) that is close to that of 20% Pt–C, while onset potential of Pd-CNHs, Pd-BCNHs and Pd-NCNHs shift negatively to −0.15 V, −0.08 V and −0.10 V, respectively. Besides, the half-wave potential E$_{1/2}$ of Pd-CNHs, Pd-BCNHs, Pd-NCNHs, Pd-NBCNHs and 20% Pt–C are determined to be −0.229 V, −0.195 V, −0.203 V, −0.152 V and −0.167 V, respectively. The positive shift of onset and half-wave potential indicate that Pd-NBCNHs displays comparable catalytic activity to that of 20% Pt–C and is able to significantly reduce the overpotential for ORR than Pd-CNHs, Pd-BCNHs and Pd-NCNHs. Though the BET surface area of Pd-NBCNHs (296.9 m^2 g^{-1}) in Fig. 6A is smaller than that of Pd-CNHs (672.5 m^2 g^{-1}),[40] Pd-BCNHs (341.7 m^2 g^{-1})[40] and Pd-NCNHs (505.9 m^2 g^{-1}),[40] its electrocatalytic performance is still superior to that of Pd-CNHs, Pd-BCNHs and Pd-NCNHs, indicating that a larger surface area does not always produce better catalytic activity and current density. The similar argument also has been reported in the study for Pd@CN catalysing ethanol electrooxidation.[41] In this work, we infer that the larger average pore size of Pd-NBCNHs (5.16 nm) in Fig. 6B could yield easier mass transportation and consequently show better performance for ORR than that of Pd-BCNHs (4.30 nm),[40] Pd-NCNHs (4.05 nm)[40] and Pd-CNHs (3.73 nm).[40] Pd NPs combined with carbon nanomaterials have been reported in the previous articles.[19–21] It is notable that the material in this work exhibits higher ORR activity about onset potential than the composites reported before (Table 1), suggesting that Pd-NBCNHs is a good choice in fuel cells operated in alkaline media.

LSV curves of the samples at various rotation speeds from 500 to 2500 rpm were measured to obtain more information about ORR kinetics and calculate the electron transfer numbers per O$_2$ during the ORR process (Fig. 7A–D). Koutecky–Levich (K–L) equation of all samples showed good linearity between j^{-1} and $\omega^{-1/2}$ in Fig. 7E. On the basis of K–L equation[19] and the slopes of these K–L plots at −0.4 V, the electron transferred numbers per O$_2$ of Pd-CNHs, Pd-BCNHs, Pd-NCNHs and Pd-NBCNHs are determined to be close to 4. The result suggests the efficient reduction of O$_2$ to H$_2$O for Pd-XCNHs (X = N, B or NB) via the desired four-electron pathway.[4,50]

To evaluate the stability of Pd-NBCNHs, I–t chronoamperometry measurement was performed. As shown in Fig. 8A, Pd-NBCNHs still retains 95.3% of its initial current after 9000 s, demonstrating a much better stability of Pd-NBCNHs than that of 20% Pt–C, which lose more than 48%. The good

Table 1 Comparison on catalytic activity of Pd-NBCNHs and other materials

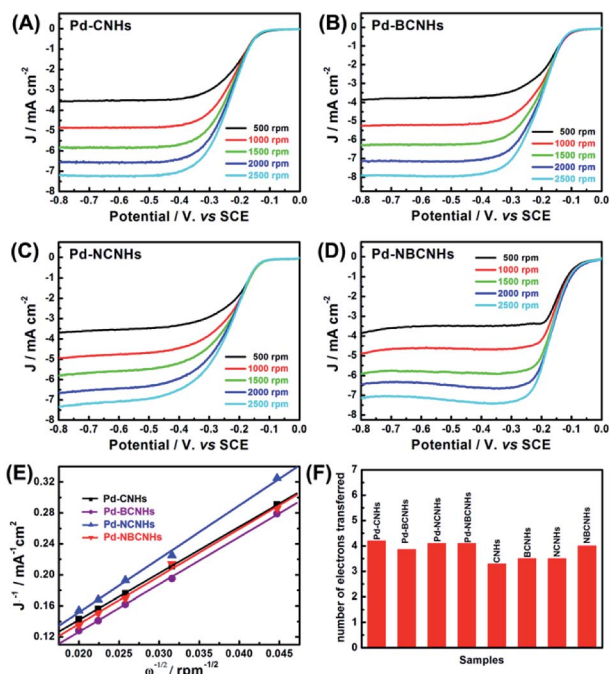| Sample	Pd-NBCNHs	G-AuPd@Pd[19]	Pd/PEDOT/rGO[21]	ER/Pd–Co-tGO[20]
Pd content (wt%)	4.70	78.0	17.3	7.75
Onset potential (V, vs. SCE)	−0.010	0.046	−0.0293	−0.146

Fig. 7 RDE voltammograms of (A) Pd-CNHs, (B) Pd-BCNHs, (C) Pd-NCNHs and (D) Pd-NBCNHs in O_2-saturated 0.1 M KOH solution at 10 mV s^{-1} with the various rotating speeds; (E) Koutecky–Levich plots of j^{-1} versus $\omega^{-1/2}$ of Pd-CNHs, Pd-BCNHs, Pd-NCNHs and Pd-NBCNHs at −0.4 V; (F) the number of electrons transferred per O_2 of samples at 0.4 V.

long-term stability of Pd-NBCNHs can be attributed to the large specific area and nanospaces of NBCNHs, which can inhibit Pd nanoparticles from agglomeration (Fig. 1C) and furthermore prevents the loss of available active site during the long-timescale ORR process. Methanol tolerance of ORR electro-catalyst is one of the important factors for potential application in the direct methanol fuel cells, because methanol may cross over the membrane and damage the ORR activity of the catalyst.
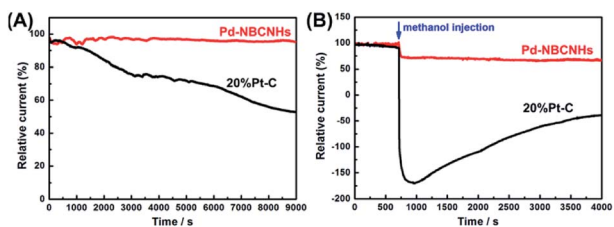

Fig. 8 (A) I−t chronoamperometry measurements of Pd-NBCNHs and 20% Pt−C at −0.3 V in O_2-saturated 0.1 M KOH solutions at a rotating rate of 1000 rpm for 9000 s; (B) methanol crossover tests of Pd-NBCNHs and 20% Pt−C at −0.3 V in O_2-saturated 0.1 M KOH solutions at a rotation rate of 1000 rpm with addition of 3 M methanol at 700 s.

With the injection of methanol (Fig. 8B), the current density of Pd-NBCNHs suffers only a small drop and then remains substantially stable, while a rapid current falloff is observed in 20% Pt–C. This result implies that Pd-NBCNHs has a much stronger tolerance to methanol crossover.

To explain the role of NBCNHs in ORR, the ORR activity of metal-free CNHs, including BCNHs, NCNHs and NBCNHs, was tested. As shown in Fig. S1,† metal-free CNHs exhibit a well-defined oxygen reduction peak in O_2-saturated 0.1 M KOH solution. In Fig. S1,† NBCNHs show a more positive peak potential (−0.245 V) compared with other metal-free CNHs (BCNHs, −0.323 V; NCNHs, −0.332 V; and CNHs, −0.358 V), indicating the increasing ORR activity in the presence of NBCNHs. In addition, the number of exchanged electrons per oxygen molecule at −0.4 V for CNHs, NCNHs, BCNHs and NBCNHs are 3.3, 3.5, 3.5 and 4.0 according to LSV curves (Fig. 9) and K–L equation, respectively. These results imply that NBCNHs are more beneficial to ORR than other single-doped CNHs or pure CNHs. It was reported that the high content of N and B atoms in the catalysts can provide oxygen adsorption sites and weaken the O–O bonds.[4,51] This is because they can induce charge redistribution to create charged sites (C^+ or B^+) for O_2 adsorption due to the different electronegativity with carbon.[36,37] Compared with NCNHs (N atoms: 1.33 at%)[40] and BCNHs (B atoms: 0.71 at%),[40] NBCNHs (the total number of N and B atoms: 2.88 at%) in this work contain more doped heteroatoms, and would derive much more charged site (C^+ and B^+) for O_2 adsorption, thereby increasing the ORR catalytic activity.

Obviously, oxygen reduction peak potential of Pd-XCNHs is more positive than that of the corresponding metal-free CNHs,
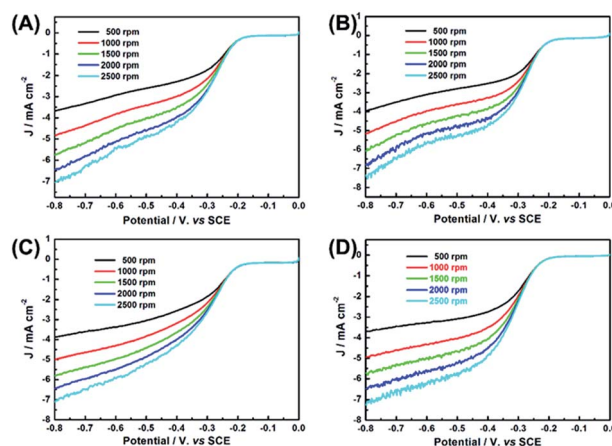

Fig. 9 RDE voltammograms of (A) CNHs, (B) BCNHs, (C) NCNHs and (D) NBCNHs in O_2-saturated 0.1 M KOH solution at 10 mV s^{-1} with the various rotating speeds.

suggesting the increased electroactivity after loading Pd NPs. The promotional effect of Pd NPs toward ORR is well known. Pd-CNHs (4.69 wt% of Pd),[40] Pd-BCNHs (4.60 wt% of Pd),[40] Pd-NCNHs (4.75 wt% of Pd)[40] and Pd-NBCNHs (4.70 wt%) have a nearly equivalent proportion of Pd. However, Pd-NBCNHs displays the highest activity while Pd-CNHs shows the poorest performance among Pd-XCNHs. The superior ORR activity of Pd-NBCNHs can be ascribed to the following factors: (i) synergetic effects between Pd NPs and NBCNHs lead to enhanced catalytic activity for ORR. NBCNHs, having much more pyrrolic N (73.34% pyrrolic N in NBCNHs; 39.28% pyrrolic N in NCNHs) that is effective to ORR as well as charged sites (B^+) caused by charge redistribution,[4,51] on the one hand play a role as a support for Pd NPs, and on the other hand serve as catalytic active sites for ORR. (ii) The larger pore size distribution of Pd-NBCNHs can generate easier mass transportation of reactants, resulting in better electrocatalytic activity for ORR than other composite materials. (iii) Compared with other catalysts (Pd-CNHs ($I_D/I_G = 1.06$),[40] Pd-BCNHs ($I_D/I_G = 1.17$)[40] and Pd-NCNHs ($I_D/I_G = 1.20$)[40]), the more defective carbon in Pd-NBCNHs ($I_D/I_G = 1.26$) can facilitate the adsorption of oxygen molecules and breakage of O–O bond, thus improve the ORR activity.[52] The disordered and defective carbon are more susceptible to the adsorption of oxygen molecule than the well-ordered structure of graphite.[53] Pd-XCNHs exhibit different catalytic activities on the onset potential, which indicates to some extent that there is a direct relationship between the electrocatalytic activity and the structural irregularities. Therefore, NBCNHs with the defective and irregular structures are suitable for electrocatalyst carriers, which provides a new strategy for exploring catalyst carriers.

Conclusions

In summary, we have successfully synthesized Pd NPs with a diameter of 2–4 nm dispersed uniformly on doped CNHs via one-step reduction method. As-prepared Pd-NBCNHs has a larger pore size distribution, more pyrrolic N and defective carbon structures than that of Pd-CNHs, Pd-BCNHs and Pd-NCNHs. Among all the catalysts, Pd-NBCNHs exhibits the highest catalytic activity for ORR and its onset potential approaches to that of commercial 20% Pt–C owing to the synergistic effect between metal palladium and NBCNHs. Because of possessing lots of pyrrolic N, charged B^+ sites and defect carbon structures, NBCNHs not only act as a carrier for Pd NPs, but also provide the active sites for oxygen adsorption on the surface of the catalyst. In addition, Pd-NBCNHs shows good long-term stability and resistance to methanol for ORR in alkaline media, which enables it to be a candidate for fuel cell.

Conflicts of interest

There are no conflicts to declare.

Acknowledgements

Notes and references

1 Y. Wang, K. S. Chen, J. Mishler, S. C. Cho and X. C. Adroher, *Appl. Energy*, 2011, **88**, 981.

2 M. S. Dresselhaus and I. L. Thomas, *Nature*, 2001, **414**, 332.

3 M. Shao, Q. Chang, J.-P. Dodelet and R. Chenitz, *Chem. Rev.*, 2016, **116**, 3594.

4 L. Dai, Y. Xue, L. Qu, H.-J. Choi and J.-B. Baek, *Chem. Rev.*, 2015, **115**, 4823.

5 S. Guo, S. Zhang and S. Sun, *Angew. Chem., Int. Ed.*, 2013, **52**, 8526.

6 T. Wang, J. Zhuo, Y. Chen, K. Du, P. Papakonstantinou, Z. Zhu, Y. Shao and M. Li, *ChemCatChem*, 2014, **6**, 1877.

7 J. Lai, B. Huang, Y. Tang, F. Lin, P. Zhou, X. Chen, Y. Sun, F. Lv and S. Guo, *Chem*, 2018, **4**, 1153.

8 Z. Chen, D. Higgins, A. Yu, L. Zhang and J. Zhang, *Energy Environ. Sci.*, 2011, **4**, 3167.

9 M. Shao, *J. Power Sources*, 2011, **196**, 2433.

10 M. H. Seo, S. M. Choi, H. J. Kim and W. B. Kim, *Electrochem. Commun.*, 2011, **13**, 182.

11 O. Savadogo, K. Lee, K. Oishi, S. Mitsushima, N. Kamiya and K.-I. Ota, *Electrochem. Commun.*, 2004, **6**, 105.

12 F. I. Pires and H. M. Villullas, *Int. J. Hydrogen Energy*, 2012, **37**, 17052.

13 E. Negro, K. Vezzù, F. Bertasi, P. Schiavuta, L. Toniolo, S. Polizzi and V. D. Noto, *ChemElectroChem*, 2014, **1**, 1359.

14 Md. R. Miah, J. Masud and T. Ohsaka, *Electrochim. Acta*, 2010, **56**, 285.

15 N. N. Kariuki, X. Wang, J. R. Mawdsley, M. S. Ferrandon, S. G. Niyogi, J. T. Vaughey and D. J. Myers, *Chem. Mater.*, 2010, **22**, 4144.

16 D. J. You, S.-a Jin, K. H. Lee, C. Pak, K. H. Choi and H. Chang, *Catal. Today*, 2012, **185**, 138.

17 X. Wang, D. Liu, S. Song and H. Zhang, *J. Am. Chem. Soc.*, 2013, **135**, 15864.

18 C. Tan, X. Huang and H. Zhang, *Mater. Today*, 2013, **16**, 29.

19 J.-N. Zheng, S.-S. Li, X. Ma, F.-Y. Chen, A.-J. Wang, J.-R. Chen and J.-J. Feng, *J. Power Sources*, 2014, **262**, 270.

20 M. Yun, M. S. Ahmed and S. Jeon, *J. Power Sources*, 2015, **293**, 380.

21 J. E. Choe, M. Shamsuddin and A. S. Jeon, *J. Power Sources*, 2015, **281**, 211.

22 T. J. Davies, M. E. Hyde and R. G. Compton, *Angew. Chem., Int. Ed.*, 2005, **44**, 5121.

23 C. E. Banks, A. Crossley, C. Salter, S. J. Wilkins and R. G. Compton, *Angew. Chem., Int. Ed.*, 2006, **45**, 2533.

24 Y. Zhao, L. Yang, S. Chen, X. Wang, Y. Ma, Q. Wu, Y. Jiang, W. Qian and Z. Hu, *J. Am. Chem. Soc.*, 2013, **135**, 1201.

25 S. Wang, E. Iyyamperumal, A. Roy, Y. Xue, D. Yu and L. Dai, *Angew. Chem., Int. Ed.*, 2011, **50**, 11756.

26 C. H. Choi, M. W. Chung, H. C. Kwon, S. H. Parka and S. I. Woo, *J. Mater. Chem. A*, 2013, **1**, 3694.

27 Y. Zheng, Y. Jiao, L. Ge, M. Jaroniec and S. Z. Qiao, *Angew. Chem., Int. Ed.*, 2013, **52**, 3110.

28 J.-i. Ozaki, N. Kimura, T. Anahara and A. Oya, *Carbon*, 2007, **45**, 1847.

29 C. H. Choi, S. H. Park and S. I. Woo, *J. Mater. Chem.*, 2012, **22**, 12107.

30 D. von Deak, E. J. Biddinger, K. A. Luthman and U. S. Ozkan, *Carbon*, 2010, **48**, 3635.

31 W. Zhang, S. Zhu, R. Luque, S. Han, L. Hu and G. Xu, *Chem. Soc. Rev.*, 2016, **45**, 715.

32 Y. Tao, D. Noguchi, C.-M. Yang, H. Kanoh, H. Tanaka, M. Yudasaka, S. Iijima and K. Kaneko, *Langmuir*, 2007, **23**, 9155.

33 S. Zhu and G. Xu, *Nanoscale*, 2010, **2**, 2538.

34 Z. Zhang, S. Han, C. Wang, J. Li and G. Xu, *Nanomaterials*, 2015, **5**, 1732.

35 X. Wu, L. Cui, P. Tang, Z. Hu, D. Ma and Z. Shi, *Chem. Commun.*, 2016, **52**, 5391.

36 L. Yang, S. Jiang, Y. Zhao, L. Zhu, S. Chen, X. Wang, Q. Wu, J. Ma, Y. Ma and Z. Hu, *Angew. Chem., Int. Ed.*, 2011, **50**, 7132.

37 S. Ni, Z. Li and J. Yang, *Nanoscale*, 2012, **4**, 1184.

38 X. Wu, L. Liu, P. Tang, M. Li and Z. Shi, *RSC Adv.*, 2016, **6**, 63730.

39 N. Li, Z. Wang, K. Zhao, Z. Shi, Z. Gu and S. Xu, *Carbon*, 2010, **48**, 1580.

40 X. Tan, X. Wu, Z. Hu, M. Ding and Z. Shi, *RSC Adv.*, 2017, **7**, 29985.

41 Y. Yan, X. Jia and Y. Yang, *Catal. Today*, 2016, **259**, 292.

42 F. Wolfers, *C. R. Hebd. Seances Acad. Sci.*, 1923, **177**, 75.

43 C. Poonjarernsilp, N. Sano, T. Charinpanitkul, H. Mori, T. Kikuchi and H. Tamon, *Carbon*, 2011, **49**, 4920.

44 J. Zheng, T. C. Ekstrom, S. K. Gordeev and M. Jacob, *J. Mater. Chem.*, 2000, **10**, 1039.

45 D. Y. Kim, C.-M. Yang, H. Noguchi, M. Yamamoto, T. Ohba, H. Kanoh and K. Kaneko, *Carbon*, 2008, **46**, 611.

46 Z.-H. Sheng, H.-L. Gao, W.-J. Bao, F.-B. Wang and X.-H. Xia, *J. Mater. Chem.*, 2012, **22**, 390.

47 H. Jin, T. Xiong, Y. Li, X. Xu, M. Li and Y. Wang, *Chem. Commun.*, 2014, **50**, 12637.

48 J. Zhu, C. He, Y. Li, S. Kang and P. K. Shen, *J. Mater. Chem. A*, 2013, **1**, 14700.

49 J.-i. Ozaki, T. Anahara, N. Kimura and A. Oya, *Carbon*, 2006, **44**, 3358.

50 S. Basu, *Recent Trends in Fuel Cell Science and Technology*, New Delhi, 2007.

51 C. H. Choi, M. W. Chung, S. H. Park and S. I. Woo, *Phys. Chem. Chem. Phys.*, 2013, **15**, 1802.

52 L. P. Zhang, Q. Xu, J. Niu and Z. Xia, *Phys. Chem. Chem. Phys.*, 2015, **17**, 16733.

53 A. Eftekhari and H. Garcia, *Materials Today Chemistry*, 2017, **4**, 1.